Rheology of Organoclay Nanocomposites: Effects of Polymer Matrix/Organoclay Compatibility and the Gallery Distance of Organoclay

Kyung Min Lee and Chang Dae Han*

Department of Polymer Engineering, The University of Akron, Akron, Ohio 44325

Received June 2, 2003

ABSTRACT: The linear dynamic viscoelasticity, and transient and intermittent shear flows of organoclay nanocomposites, which were prepared with poly(ethylene-*ran*-vinyl acetate) (EVA), poly(ethylene-*ran*-vinyl alcohol) having 53 mol % vinyl alcohol (EVOH-53), or poly(ethylene-*ran*-vinyl acetate-*ran*-vinyl alcohol) having 5 mol % vinyl alcohol (EVAOH-5) were investigated. For the study, two organoclays (Southern Clay Products) were employed: (i) Cloisite 30B (having the gallery distance of 1.85 nm) treated with a surfactant (MT2EtOH) containing tallow, quaternary ammonium chloride, and hydroxyl groups and (ii) Cloisite 15A (having the gallery distance of 3.15 nm) treated with a surfactant (2M2HT) containing hydrogenated tallow, quaternary ammonium chloride but no hydroxyl group. Thus, a total of six nanocomposites were prepared by melt blending using a Brabender mixer. Before taking rheological measurements, the nanocomposites were characterized using X-ray diffraction (XRD) and transmission electron microscopy (TEM). The linear dynamic viscoelastic measurements indicate that the dynamic storage modulus of the (EVAOH-5)/Cloisite 30B and EVA/Cloisite 15A nanocomposites increased as the temperature increased from 120 to 180 °C, while the dynamic storage modulus of the (EVAOH-5)/Cloisite 15A and EVA/Cloisite 30B nanocomposites decreased with increasing temperature. The intermittent shear flow experiments indicate that structural reorganization occurred, during the rest period upon cessation of the initial transient, in the (EVAOH-5)/Cloisite 30B and EVA/Cloisite 15A nanocomposites, while there was very little evidence of such for the (EVAOH-5)/Cloisite 15A and EVA/Cloisite 30B nanocomposites. The unusual rheological observations made in this study are explained in terms of the compatibility between the polymer matrix and organoclay and the gallery distance of organoclay. In-situ Fourier transform infrared spectroscopy indicates that EVAOH-5 and Cloisite 30B, which both have hydroxyl groups, formed hydrogen bonds even at 180 °C, the highest experimental temperature employed, while little evidence was found indicating the formation of hydrogen bonds between EVAOH and Cloisite 15A.

1. Introduction

During the past decade, a large number of research groups have reported on the preparation, characterization, and rheological or mechanical properties of layered silicate nanocomposites based on thermoplastic polymers. There are too many papers (hundreds) to cite them all here. The readers are referred to recent review articles[1−4] and a recent paper by Sur et al.,[5] who cited 206 references.

When a thermoplastic polymer is mixed with layered silicates, it either intercalates or exfoliates the layered silicates. From the point of view of obtaining markedly improved physical/mechanical properties of nanocomposites, exfoliation is preferred to intercalation. In general, intercalation is observed when a polymer matrix and layered silicates do not have sufficient attractive interactions, while exfoliation is observed when a polymer matrix and layered silicates have strong attractive interactions. Then, as in the preparation of miscible polymer blends, compatibility between layered silicates and polymer matrix is necessary to achieve a high degree of exfoliation of layered silicate aggregates and thus improved physical/mechanical properties of nanocomposites. Thus, a fundamental issue in the preparation of nanocomposites is how to provide strong attractive interactions between layered silicates and polymer matrix. Over the past decade much effort has been spent on a better understanding of intercalation and exfoliation in the preparation of nanocomposites. Thermodynamic aspects of intercalation and exfoliation in nanocomposites have been investigated.[6−11]

In a previous paper,[12] we reported that the nanocomposites composed of a polystyrene-*block*-hydroxylated polyisoprene copolymer and an organoclay treated with a surfactant having hydroxyl groups formed hydrogen bonds during mixing and gave rise to a high degree of exfoliation of organoclay aggregates. In a subsequent paper,[13] we reported that the nanocomposites composed of polycarbonate having carbonyl groups and an organoclay treated with a surfactant having hydroxyl groups also formed hydrogen bonds during melt blending, which resulted in a high degree of exfoliation of organoclay aggregates. The above experimental results were interpreted in terms of an enhanced compatibility, via hydrogen bonding, between polymer matrix and organoclay since it is well established that specific interactions via hydrogen bonding enhances the compatibility of a polymer pair.[14]

Specific interactions such as ionic interactions, dipole−dipole interactions, and the formation of electron donor−acceptor complexes can also provide attractive interactions between layered silicates and polymer matrix. Indeed, some research groups[15−18] prepared layered silicate nanocomposites, in which the majority of the polymer chains are tethered to the surface of the layered silicates. When chemical modification of a thermoplastic polymer, chosen for mixing with an organoclay, is not possible, one can use a third component as a compatibilizing agent. One good example of such practice is the use of maleated polypropylene (PP) in the preparation of nanocomposites composed of PP and organoclay. Some research groups[19−23] used such an approach to prepare organoclay nanocomposites based on PP. Nano-

10.1021/ma030302w CCC: $25.00
Published on Web 08/29/2003

composites have been prepared from a number of other thermoplastic polymers, besides PP: polyamides (nylon),[17,24−28] polystyrene,[29−32] poly(ethylene oxide),[33−35] poly(L-lactide),[36] poly(vinylpyridine),[37] poly(ϵ-caprolactone),[15−17,38−40] poly(ethylene-*ran*-vinyl acetate),[41−44] and polysulfone.[5] The list given above is by no means exhaustive.

Although many research groups have reported on the rheological behavior of different nanocomposites, there does not seem to be a systematic study which addressed the very fundamental issue of the compatibility between polymer matrix and organoclay. The rheological behavior of nanocomposites depends on the degree of dispersion of organoclay aggregates (i.e., morphology), which in turn depends, among many factors, on the degree of compatibility between polymer matrix and organoclay, as is the case for polymer blends. In addition, the gallery distance of organoclay should also play an important role in determining the degree of exfoliation of organoclay aggregates. What determines the gallery distance of organoclay is the chemistry of the surfactant that is applied to the surface of pristine layered silicates. Note that layered silicates have a large active surface area (700−800 m^2/g in the case of montmorillonite) and a moderate negative surface charge (cation exchange capacity). Upon replacing the hydrated metal cation from the interlayers of the pristine layered silicates with organic cations such as an alkyammonium, the layered silicate attains a hydrophobic/organophilic character, which typically results in large interlayer spacing. Because the negative charge originates in the layered silicate, the cationic head groups of the alkylammonium chloride molecule preferentially reside at the surface of the layered silicate (i.e., the quaternary ammonium chloride portion of the surfactants, for example, interact with the silicate surface), while the oligomeric tallow species, which sometime contain polar groups, extend into the galleries. Therefore, it is very important to match the chemical affinity between a polymer matrix and an organoclay in order to achieve a very high degree of exfoliation of organoclay platelets in a polymer matrix.

In this study, we have investigated the rheology of organoclay nanocomposites by choosing two organoclays: one treated with a surfactant having polar groups and another treated with a surfactant having no polar groups. The two organoclays chosen have different gallery distances, which enabled us to assess the importance of the gallery distance of an organoclay *relative* to the degree of compatibility between polymer matrix and the organoclay. For the study we have chosen three thermoplastic polymers: poly(ethylene-*ran*-vinyl acetate) (EVA), poly(ethylene-*ran*-vinyl alcohol) (EVOH), and poly(ethylene-*ran*-vinyl acetate-*ran*-vinyl alcohol) (EVAOH). The rationale behind the choice of these polymers was the following. EVA is a *nonpolar* random polymer, while EVOH is a *polar* random polymer that can be obtained by 100% alcoholysis (or hydrolysis) of the vinyl acetate in EVA. We were able to control the degree of polarity by partial hydrolysis of EVA, which yields the terpolymer EVAOH. Thus, in this study we were able to investigate the rheological behavior of nanocomposites composed of an organoclay (nonpolar or partly polar) and a polymer matrix having a wide range of polarity from nonpolar EVA to highly polar EVOH. Since it is generally accepted that an increased polarity of polymer matrix increases its compatibility with, and affinity for, polar surfaces of organoclay, the organoclays and thermoplastic polymers chosen in the present study enabled us to conduct a systematic investigation on the effects of polymer matrix/organoclay compatibility and the gallery distance of organoclay on the rheological behavior of the nanocomposites prepared. The nanocomposites were characterized using X-ray diffraction (XRD), transmission electron microscopy (TEM), and Fourier transform infrared (FTIR) spectroscopy, before rheological measurements were made. Then we investigated the linear dynamic viscoelasticity and transient/intermittent shear flow behavior of the nanocomposites prepared, with emphasis on the effects of polymer/matrix compatibility and the gallery distance of organoclay. In this paper we report the highlights of our findings from this study.

Table 1. Molecular Characteristics of EVA, EVAOH, and EVOH Employed in This Study

sample code	M_n (g/mol)	M_w/M_n[a]	VA or VOH (mol %)[b]
EVA	1.23×10^5 [a]	1.08	19 (VA)
EVAOH-5	1.23×10^5 [c]		5 (VOH)
EVOH-53	NA[d]	NA[d]	53 (VOH)

[a] Determined from GPC. [b] Determined from FTIR. [c] Calculated from stoichiometry. [d] Unable to determine owing to partial solubility in THF.

2. Experimental Section

Materials and Preparation of Nanocomposites. In the present study, EVA, EVOH, and EVAOH were used to prepare nanocomposites with an organoclay. Specifically, a laboratory grade of EVA (19 mol % VA) purchased from Aldrich was used, and a commercial grade of EVOH (G156, EVAL Company of America) having 53 mol % vinyl alcohol (VOH) was used (which will be referred to as EVOH-53). Having found that EVOH-53 had too high a content of hydroxyl groups to effectively disperse organoclay aggregates during melt blending, the reason for which will be elaborated on below, we prepared an EVAOH, via partial hydrolysis of the EVA purchased from Aldrich, having 5 mol % vinyl alcohol in the terpolymer (below, this terpolymer will be referred to as EVAOH-5) by following the procedures described in the literature.[45,46] Briefly described, a predetermined amount of EVA was slowly added to a boiling mixed solvent (84 °C) of 500 mL of benzene and 500 mL of 2-propanol under an argon atmosphere and dissolved in a single-necked 2500 mL flask with a reflux condenser. The reaction mixture was dissolved completely at 84 °C under an argon atmosphere, and then a predetermined amount of potassium hydroxide (KOH) was added to the reaction mixture. After the hydrolysis reaction was run for 72 h, the temperature was lowered to 64 °C. Then 100 mL of 2-propanol was added to the reaction mixture, and subsequently the organic solvent was decanted. The partially hydrolyzed EVAOH-5 was washed with water several times to remove the remaining salt and base, potassium acetate (KOAc) and KOH, respectively. The terpolymer was dried for 48 h at 64 °C in a vacuum oven. Table 1 gives the molecular characteristics of EVA, EVAOH-5, and EVOH-53.

In this study we employed two commercial organoclays (Southern Clay Products): (i) Cloisite 30B treated with a surfactant (MT2EtOH) having the chemical structure: methyl, tallow, bis(2-hydroxyethyl), quaternary ammonium chloride[47]

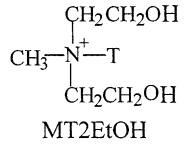

MT2EtOH

where N^+ denotes quaternary ammonium chloride and T denotes tallow consisting of ca. 65% C18, ca. 30% C16, and

Table 2. Chemical Structure of Surfactant and the Mean Interlayer Spacing (d_{001}) of Organoclays Available from Southern Clay Products

sample code	chemical structure of surfactant	d_{001} (nm)
Cloisite 30B	methyl, tallow, bis-2-hydroxyethyl, quaternary ammonium chloride, MT2EtOH	1.85
Cloisite 6A	dimethyl, didydrogenated tallow, quaternary ammonium chloride, 2M2HT	3.51
Cloisite 10A	dimethyl, benzyl, hydrogenated tallow, quaternary ammonium chloride, 2MBHT	1.92
Cloisite 15A	dimethyl, dihydrogenated tallow, quaternary ammonium chloride, 2M2HT	3.15
Cloisite 20A	dimethyl, dihydrogenated tallow, quaternary ammonium chloride, 2M2HT	2.42
Cloisite 25A	dimethyl, dihydrogenated tallow, 2ethylhexyl quaternary ammonium, 2MHTL8	1.86
Cloisite 93A	dimethyl, dihydrogenated tallow, ammonium, M2HT	2.36

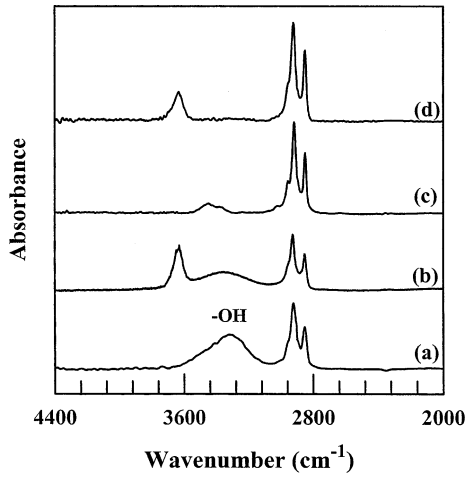

Figure 1. FTIR spectra for (a) surfactant MT2EtOH, (b) Cloisite 30B, (c) surfactant 2M2HT, and (d) Cloisite 15A.

ca. 5% C14 and (ii) Cloisite 15A treated with a surfactant (2M2HT) having the chemical structure: methyl, hydrogenated tallow, quaternary ammonium chloride[47]

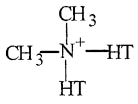

2M2HT

where N^+ denotes quaternary ammonium chloride and HT denotes hydrogenated tallow consisting of ca. 65% C18, ca. 30% C16, and ca. 5% C14. It should be mentioned that 100% of Na^+ ions in natural montmorillonite have been exchanged. The FTIR spectra for MT2EtOH, Cloisite 30B, 2M2HT, and Cloisite 15A are given in Figure 1, in which the absorption band at ca. 3360 cm^{-1} represents the hydroxyl (−OH) group. It is clearly seen in Figure 1 that both MT2EtOH and Cloisite 30B have the −OH group and that the area under the absorption band at ca. 3360 cm^{-1} for Cloisite 30B is much smaller. This is reasonable because the amount of MT2EtOH in Cloisite 30B is ca. 32%. On the other hand, in Figure 1 we observe no evidence of the −OH group present in 2M2HT and Cloisite 15A. The rationale behind the choice of the two organoclays, Cloisite 30B and Cloisite 15A, in this study lies in that among the several organoclays available from Southern Clay Products, as summarized in Table 2, Cloisite 30B is the only one that has hydroxyl groups, while the gallery distance of Cloisite 15A is much larger than that of Cloisite 30B. Therefore, we chose Cloisite 30B and Cloisite 15A in order to investigate (i) the effect of hydroxyl groups in Cloisite 30B when it is mixed with EVOH-53 or EVAOH-5 and (ii) the effect of the difference in gallery distance between Cloisite 15A and Cloisite 30B when each is mixed with EVOH-53, EVAOH-5, or EVA on the degree of intercalation or exfoliation of organoclay aggregates in the respective nanocomposites.

In this study, nanocomposites were prepared by melt blending Cloisite 30B or Cloisite 15A with EVA, EVOH-53, or EVAOH-5 using a Brabender mixer. The amount of organoclay in each nanocomposite was 5 wt %. Hereafter, we will not mention further the composition of each nanocomposite when presenting our experimental results below, since only one composition was employed in this study. The following melt blend conditions were employed for the different nanocomposite systems. In the preparation of EVA/organoclay and (EVAOH-5)/organoclay nanocomposites the Brabender mixer was operated at 120 °C and 60 rpm for 15 min, and in the preparation of (EVOH-53)/organoclay nanocomposite the Brabender mixer was operated at 180 °C and 60 rpm for 15 min. The melt blended nanocomposites were dried in a vacuum oven and then stored at low temperature. Table 3 gives a summary of sample codes of the nanocomposites prepared. The specimens for rheological measurements were prepared by compression molding of the dried nanocomposites at the same temperature as that employed for melt blending.

Table 3. Summary of Sample Codes of the Nanocomposites Investigated in This Study

sample code	description
EVA	laboratory grade (19 mol % VA)
EVA/Cloisite 30B	5 wt % Cloisite 30B
EVA/Cloisite 15A	5 wt % Cloisite 15A
EVAOH-5	partially hydrolyzed (5 mol % VOH)
(EVAOH-5)/Cloisite 30B	5 wt % Cloisite 30B
(EVAOH-5)/Cloisite 15A	5 wt % Cloisite 15A
EVOH-53	commercial grade (53 mol % VOH)
(EVOH-53)/Cloisite 30B	5 wt % Cloisite 30B
(EVOH-53)/Cloisite 15A	5 wt % Cloisite 15A

X-ray Diffraction (XRD). Using a Rigaku X-ray generator operated at 50 kV and 100 mA, XRD patterns were obtained to determine the mean interlayer spacing of the (001) plane (d_{001}) for all six nanocomposites prepared. The X-ray beam was monochromatized to Cu Kα with a graphite crystal. The range of 2θ scanning of X-ray intensity employed was 1.5°−10°.

Transmission Electron Microscopy (TEM). TEM images of all nanocomposite specimens without staining were taken at room temperature using a transmission electron microscope (JEM1200EX 11, JEOL) operated at 120 kV. The ultrathin sectioning (50−70 nm) was performed at room temperature for (EVOH-53)/Cloisite 15A and (EVOH-53)/Cloisite 30B nanocomposites and at −60 °C for EVA/Cloisite 30B, (EVAOH-5)/Cloisite 30B, and (EVAOH-5)/ Cloisite 15A nanocomposites using a Reichert Ultracut E low-temperature sectioning system.

Fourier Transform Infrared (FTIR) Spectroscopy. Using a Fourier transform infrared spectrometer (16 PC FTIR, Perkin-Elmer), FTIR spectra were obtained at room temperature for EVA, EVAOH-5, EVAOH-11, and EVOH-53. To observe variations in the height of the absorption band at about 3360 cm^{-1}, representing the −OH group, with the degree of hydrolysis of EVA, we prepared an additional terpolymer, EVAOH-11 having 11 mol % VOH. Spectral resolution was maintained at 4 cm^{-1}. Dry argon gas was used to purge the sample compartment in order to reduce the interference of water and carbon dioxide in the spectrum. Since no suitable solvent could be found for EVOH-53, thin films of (EVOH-53)/organoclay nanocomposites were prepared by compression molding to obtain FTIR spectra. For all other nanocomposites prepared in this study thin films were prepared by casting 2% (w/v) solution in THF directly on the KBr salt plate to obtain FTIR spectra. Film thickness was adjusted, such that the maximum absorbance of any band was less than 1.0, at which the Beer−Lambert law is valid. Samples were then stored under vacuum until use. Figure 2 gives FTIR spectra for EVA,

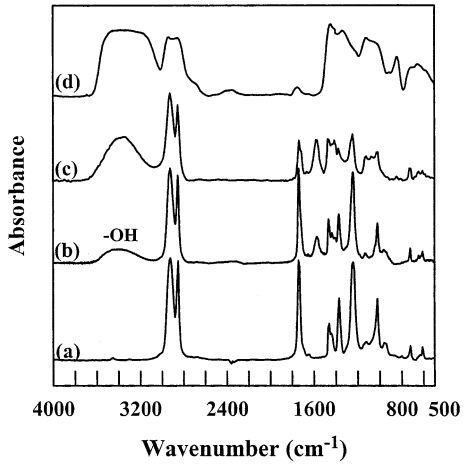

Figure 2. FTIR spectra for (a) EVA, (b) EVAOH-5, (c) EVAOH-11, and (d) EVOH-53 taken at room temperature.

EVAOH-5, EVAOH-11, and EVOH-53 specimens. The assignments of various IR absorption bands in EVAOH can be found in the literature.[45] The broad absorption band centered at ca. 3360 cm^{-1}, representing the hydroxyl (−OH) group, is the most important one. The disappearance of the absorption band at ca. 610 cm^{-1} has been used for quantitative determination of VA content in an EVAOH.[45] It is seen in Figure 2 that the absorption band at ca. 3360 cm^{-1} decreases as the degree of hydrolysis of EVA is decreased from 11 mol % (EVAOH-11) to 5 mol % (EVAOH-5). According to Koopmans et al.,[45] the absorption band at ca. 720 cm^{-1}, which remains unchanged after partial hydrolysis, may also be used to determine the VA content in an EVAOH.

Rheological Measurements. An Advanced Rheometric Expansion System (ARES, Rheometric Scientific) with a parallel-plate fixture (25 mm diameter) was used to conduct dynamic frequency sweep experiments of the nanocomposites, measuring the storage and loss moduli (G' and G'') as functions of angular frequency (ω) (ranging from 0.01 to 100 rad/s) and at 120−220 °C. In conducting oscillatory shear measurements, the following protocols were employed. A specimen was first placed in the parallel-plate fixture that was preheated to a predetermined experimental temperature, and then the gap setting was adjusted to about 1 mm by squeezing. After the temperature of the specimen was equilibrated, we monitored the normal force signal to make certain that it reached the baseline (i.e., zero normal force) prior to testing; squeezing of a specimen generated normal stress in the specimen. We found that the time required for the residual stress, which was generated during squeezing, to relax took a relatively short time (less than 10 min). Only after it was ascertained that the normal force signal reached the baseline did oscillatory shear experiments commence. Using such a protocol, we were able to obtain reproducible data. In the oscillatory shear measurements a fixed strain of 0.04 was used to ensure that measurements were taken well within the linear viscoelastic range of the materials investigated. The frequency sweep experiment at a preset temperature lasted for about 45 min, while temperature control was accurate to within ±1 °C. We also conducted experiments of transient shear flow, intermittent shear flow after rest for a predetermined period upon cessation of shear flow, and steady-state shear flow at different shear rates using the cone-and-plate fixture (25 mm diameter). The experimental protocols employed for the transient and steady-state shear experiments were virtually the same as that for the oscillatory shear experiments described above, except for that the gap setting of the cone-and-plate fixture was 50 μm. Only after it was ascertained that the normal force signal had reached the baseline did transient shear flow commence until steady state was reached. Using such a protocol, we were able to obtain reproducible data. All measurements were conducted under a nitrogen atmosphere to avoid oxidative degradation of the specimens.

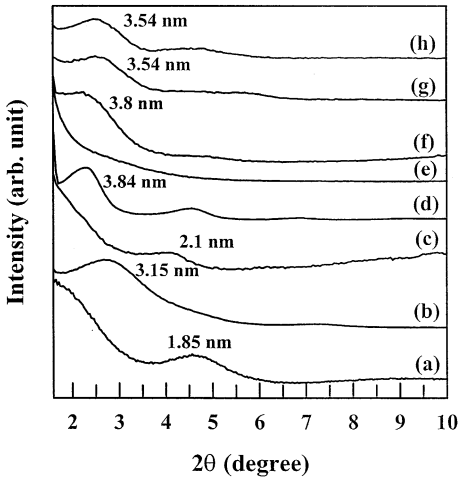

Figure 3. XRD patterns for (a) Cloisite 30B, (b) Cloisite 15A, (c) EVA/Cloisite 30B nanocomposite, (d) EVA/Cloisite 15A nanocomposite, (e) (EVAOH-5)/Cloisite 30B nanocomposite, (f) (EVAOH-5)/Cloisite 15A nanocomposite, (g) (EVOH-53)/Cloisite 30B nanocomposite, and (h) (EVOH-53)/Cloisite 15A nanocomposite.

Cloud Point Measurements. The cloud point of a specimen was determined using laser light scattering. Specifically, a slide glass containing a specimen was placed on the hot stage of the sample holder fitted with a programmable temperature controller. A low-power He−Ne laser (wavelength of 635 nm) was used as the light source, and a photodiode was used as the detector. A specimen was first heated to a temperature slightly (ca. 20 °C) above the cloud point (i.e., in the isotropic region) followed by slow cooling into the two-phase region where a change in light intensity was noticeable, and then the specimen was heated again at a preset rate (0.5−5 °C/min), during which information on both temperature and the intensity of scattered light was stored on a computer. For each composition of a particular blend system, cloud point measurements were repeated 3−5 times until data were reproducible, and a fresh specimen was used for each experimental run. For a given blend system, 8−9 compositions from 10/90 to 90/10 blend ratios were used for cloud point measurements. A plot of the intensity of scattered light vs temperature during heating was prepared, which then allowed us to construct a binodal curve, the results of which will be presented below.

3. Results

X-ray Diffraction (XRD) of Organoclay Nanocomposites Based on EVA, EVOH, or EVAOH. Figure 3 gives XRD patterns of Cloisite 30B, Cloisite 15A, and six nanocomposites. Notice in Figure 3 that Cloisite 30B has a gallery distance (d_{001} spacing) of 1.85 nm, while Cloisite 15A has a d_{001} spacing of 3.15 nm. The following observations are worth noting in Figure 3. (i) The EVA/Cloisite 30B nanocomposite has a d_{001} spacing of 2.1 nm, an increase of only 0.25 nm (13.5% increase) over the d_{001} spacing of Cloisite 30B, while the EVA/Cloisite 15A nanocomposite has a d_{001} spacing of 3.84 nm, an increase of 0.69 nm (21.9% increase) over the d_{001} spacing of Cloisite 15A. This observation seems to suggest that the degree of intercalation of the Cloisite 15A aggregates in EVA might be slightly higher than that of Cloisite 30B in EVA. (ii) The (EVAOH-5)/Cloisite 30B nanocomposite does not exhibit a discernible intensity peak, while the (EVAOH-5)/Cloisite 15A nanocomposite has a d_{001} spacing of 3.80 nm, an increase of 0.65 nm (20.6% increase) over the d_{001} spacing of Cloisite 15A. This observation seems to suggest that Cloisite 30B aggregates might have been reasonably well dispersed (exfoliated to a certain degree) in EVAOH-5, while the

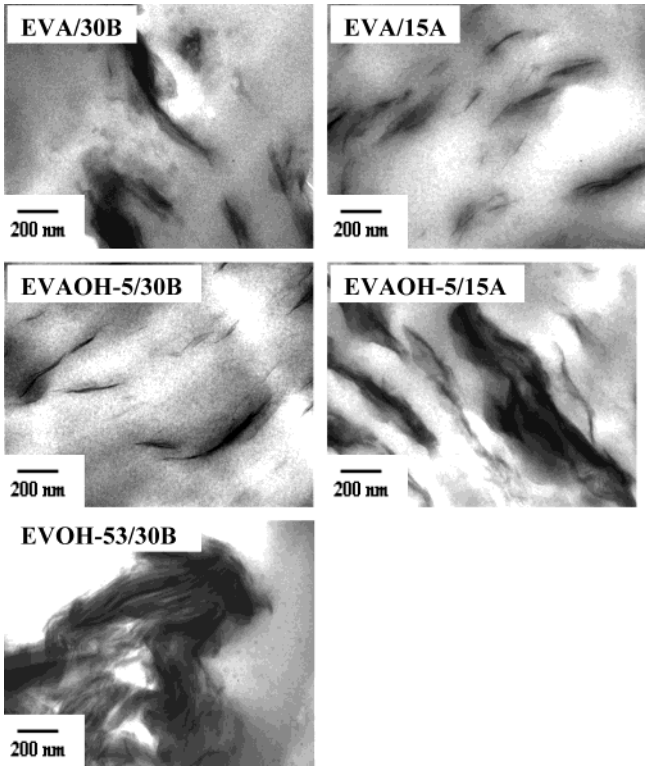

Figure 4. TEM images of EVA/Cloisite 30B nanocomposite, EVA/Cloisite 15A nanocomposite, (EVAOH-5)/Cloisite 30B nanocomposite, (EVAOH-5)/Cloisite 15A nanocomposite, and (EVOH-53)/Cloisite 30B nanocomposite.

Cloisite 15A aggregates might only be intercalated by EVAOH-5. (iii) Both (EVOH-53)/Cloisite 30B and (EVOH-53)/Cloisite 15A nanocomposites have the same d_{001} spacing of 3.54 nm, indicating that the d_{001} spacing of the (EVOH-53)/Cloisite 30B nanocomposite has increased by 1.69 nm (91% increase) over the d_{001} spacing of Cloisite 30B, while the d_{001} spacing of the (EVOH-53)/Cloisite 15A nanocomposite has increased by 0.39 nm (12.4% increase) over the d_{001} spacing of Cloisite 15A. This observation seems to suggest that the degree of intercalation of Cloisite 30B aggregates in EVOH-53 might be higher than that of Cloisite 15A aggregates in EVOH-53. (iv) The difference in XRD patterns between the (EVAOH-5)/Cloisite 30B and (EVOH-53)/Cloisite 30B nanocomposites seems to indicate that EVOH-53 was not as effective as EVAOH-5 in dispersing Cloisite 30B aggregates. Although XRD patterns may not be regarded as being the most sensitive measure for describing the degree of intercalation or exfoliation of organoclay aggregates in a polymer matrix, they certainly are very useful to make qualitative observations.

Morphology of Organoclay Nanocomposites Based on EVA, EVOH, or EVAOH. Figure 4 gives TEM images of EVA/Cloisite 30B, EVA/Cloisite 15A, (EVAOH-5)/Cloisite 30B, (EVAOH-5)/Cloisite 15A, and (EVOH-53)/Cloisite 30B nanocomposites, in which the dark areas represent the clay and the gray/white areas represent the polymer matrix. The following observations are worth noting in Figure 4. Within experimental uncertainties, the degree of intercalation of Cloisite 15A in the EVA/Cloisite 15A nanocomposite is higher than that of Cloisite 30B in the EVA/Cloisite 30B nanocomposite. This observation is consistent with that made from the XRD patterns given in Figure 3. It can be seen in Figure 4 that the degree of dispersion of Cloisite 30B aggregates in the (EVAOH-5)/Cloisite 30B nanocomposite is considerably higher than that in the (EVOH-53)/Cloisite 30B nanocomposite. A reasonably high degree of dispersion of Cloisite 30B aggregates in the (EVAOH-5)/Cloisite 30B nanocomposite is attributable to the existence of attractive interactions, via hydrogen bonding, between the hydroxyl groups in EVAOH-5 and the hydroxyl groups in the surfactant MT2EtOH residing at the surface of Cloisite 30B. Notice in Figure 4 that the very large Cloisite 30B aggregates are not even well intercalated in the (EVOH-53)/Cloisite 30B nanocomposite, suggesting that Cloisite 30B and EVOH-53 had very poor compatibility (i.e., strong repulsive interactions) although EVOH-53 has very large amounts of hydroxyl groups (53 mol %). The reason is that the attractive forces within the EVOH-53 molecules are too strong, prohibiting attractive interactions between the hydroxyl groups in EVOH-53 and the hydroxyl groups in the surfactant MT2EtOH residing at the surface of Cloisite 30B. The above observation is consistent with that made from the XRD patterns given in Figure 3. Further, in Figure 4 we observe that the degree of dispersion of organoclay aggregates in the (EVAOH-5)/Cloisite 30B nanocomposite is much higher than that in the (EVAOH-5)/Cloisite 15A nanocomposite. Again, this observation is consistent with that made from the XRD patterns given in Figure 3.

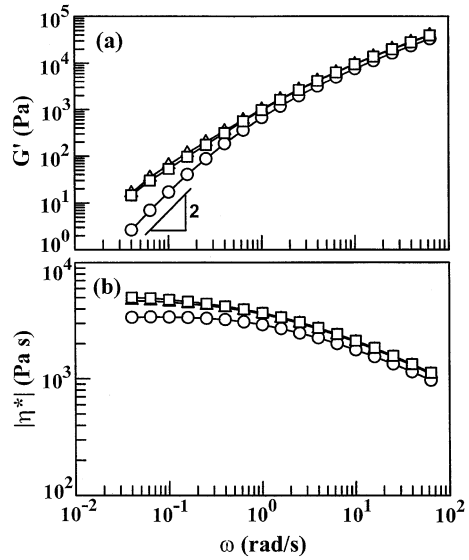

Figure 5. Plots of (a) log G' vs log ω and (b) log $|\eta^*|$ vs log ω at 180 °C for (○) EVOH-53, (△) (EVOH-53)/Cloisite 30B nanocomposite, and (□) (EVOH-53)/Cloisite 15A nanocomposite.

Linear Dynamic Viscoelasticity of Organoclay Nanocomposites Based on EVOH-53, EVAOH-5 or EVA. Figure 5 gives (a) log G' vs log ω plots and (b) log $|\eta^*|$ vs log ω plots at 180 °C for EVOH-53, (EVOH-53)/Cloisite 30B, and (EVOH-53)/Cloisite 15A nanocomposites, in which values of complex viscosity $|\eta^*|$ were calculated using $|\eta^*| = [(G'/\omega)^2 + (G''/\omega)^2]^{1/2}$. In Figure 5, no clear difference in linear dynamic viscoelasticity between the (EVOH-53)/Cloisite 30B and (EVOH-53)/Cloisite 15A nanocomposites can be discerned, and values of G' and $|\eta^*|$ in both nanocomposites are increased only slightly in the low-frequency region over those of neat EVOH-53. The above observation supports the results of the XRD patterns given in Figure 3 and the TEM images given in Figure 4 in that little or no compatibility exists between EVOH-53 and Cloisite

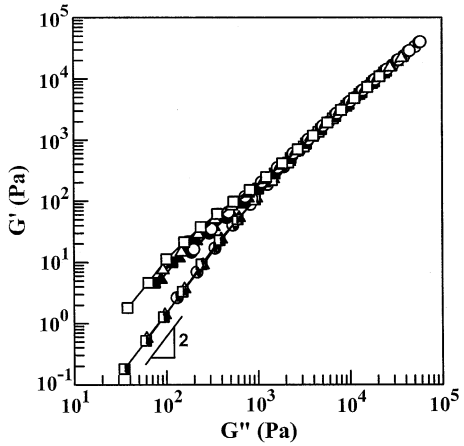

Figure 6. Plots of log G' vs log G'' for EVOH-53 at 180 (◑), 200 (▲), and 220 °C (◨); (EVOH-53)/Cloisite 15A nanocomposite at 180 (●), 200 (▲), and 220 °C (■); and (EVOH-53)/Cloisite 30B nanocomposite at 180 (○), 200 (△), and 220 °C (□).

15A and between EVOH-53 and Cloisite 30B. The readers are reminded that the *intramolecular* attractive forces (via hydrogen bonding) within EVOH-53 molecule themselves are so strong that little *intermolecular* attractive forces apparently can take place between the hydroxyl groups in EVOH-53 and the hydroxyl groups in the surfactant MT2EtOH residing at the surface of Cloisite 30B. Since Cloisite 15A was treated with surfactant 2M2HT which does not have any polar group, little or no compatibility between EVOH-53 and 2M2HT residing at the surface of Cloisite 15A is expected.

Figure 6 gives log G' vs log G'' plots at 180, 200, and 220 °C for EVOH-53, (EVOH-53)/Cloisite 30B, and (EVOH-53)/Cloisite 15A nanocomposites. In Figure 6, we observe that the log G' vs log G'' plots for EVOH-53 are independent of temperature and have a slope of 2 in the terminal region, as is expected for all ordinary linear polymers.[48,49] It is interesting to observe in Figure 6 that log G' vs log G'' plots of both (EVOH-53)/Cloisite 30B and (EVOH-53)/Cloisite 15A nanocomposites are independent of temperature and have a slope less than 2 in the terminal region. It has been found that log G' vs log G'' plots are very useful to investigate (or monitor) morphological evolution with temperature in microphase-separated block copolymers[50−52] and thermotropic liquid-crystalline polymers.[53−55] Thus, we can conclude from Figure 6 that little change in morphology occurred in the (EVOH-53)/Cloisite 30B and (EVOH-53)/Cloisite 15A nanocomposites as the temperature increased from 180 to 220 °C. This observation is not surprising since little or no attractive interactions exist between EVOH-53 and Cloisite 30B and between EVOH-53 and Cloisite 15A.

Having concluded that EVOH-53 is not compatible with the surfactant MT2EtOH residing at the surface of Cloisite 30B, although both have hydroxyl groups, we decided to prepare an EVAOH that has a sufficiently low degree of VOH by partial hydrolysis of EVA. The rationale behind this approach was that the *intramolecular* attractive forces (via hydrogen bonding) within the EVAOH molecule themselves would be less strong than in EVOH-53, which would allow *intermolecular* attractive forces between the hydroxyl groups in EVAOH and the hydroxyl groups in the surfactant MT2EtOH residing at the surface of Cloisite 30B, during mixing, thus enhancing the compatibility between EVAOH and MT2EtOH. Since we had no idea a priori as to how low

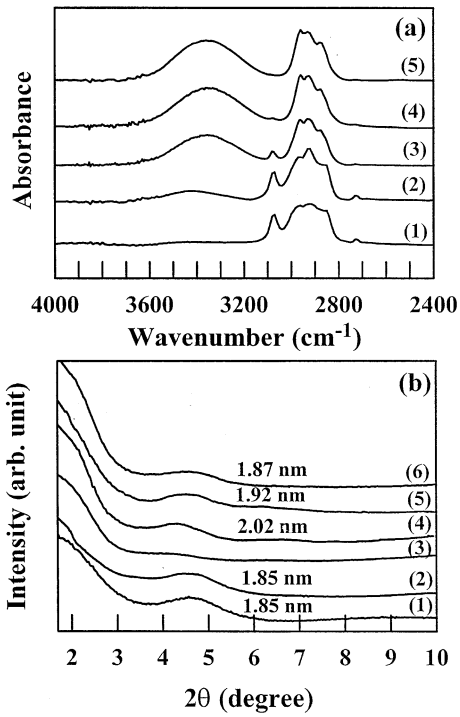

Figure 7. (a) FTIR spectra for (1) PI, (2) PIOH-30, (3) PIOH-50, (4) PIOH-75, and (5) PIOH-100. (b) XRD patterns for (1) Cloisite 30B, (2) PI/Cloisite 30B nanocomposite, (3) (PIOH-30)/Cloisite 30B nanocomposite, (4) (PIOH-50)/Cloisite 30B nanocomposite, (5) (PIOH-75)/Cloisite 30B nanocomposite, and (6) (PIOH-100)/Cloisite 30B nanocomposite.

a level of VOH we must have in a partially hydrolyzed EVAOH, we decided to prepare a series of nanocomposites composed of hydroxylated polyisoprene (PIOH) and Cloisite 30B or Cloisite 15A and then investigate their gallery distances using XRD. For this, we synthesized, via anionic polymerization, a homopolymer polyisoprene (PI) having predominantly vinyl content (3,4- and 1,2-addition microstructures) and then hydroxylated it, via hydroboration/oxidation reactions, to obtain PIOHs with varying degrees of hydroxylation (30, 50, 75, and 100%) using the procedure described in our previous paper.[56] We took this approach, instead of the hydrolysis of EVA, because neat PIOH would give us a very clear picture about the effectiveness of the level of hydroxyl groups in a nanocomposite.

Figure 7a gives the FTIR spectra for PI, PIOH-30, PIOH-50, PIOH-75, and PIOH-100, in which the numbers (30, 50, 75, and 100) refer to the percentage of hydroxylation of the vinyl content that existed in the homopolymer PI. It is seen in Figure 7a that the area under the adsorption band at ca. 3360 cm^{-1}, representing −OH group, increases with increasing degree of hydroxylation. Figure 7b gives the XRD patterns for (1) Cloisite 30B, (2) PI/Cloisite 30B, (3) (PIOH-30)/Cloisite 30B, (4) (PIOH-50)/Cloisite 30B, (5) (PIOH-75)/Cloisite 30B, and (6) (PIOH-100)/Cloisite 30B, in which the concentration of Cloisite 30B in the nanocomposites was 5 wt %. It is very interesting to observe in Figure 7 that (i) the (PIOH-30)/Cloisite 30B nanocomposite shows a very broad, almost indistinguishable intensity peak, (ii) the d_{001} spacing of the (PIOH-50)/Cloisite 30B nanocomposite is 2.02 nm, slightly higher than the d_{001} spacing (1.85 nm) of Cloisite 30B, and (iii) the d_{001} spacing of the other nanocomposites decreases with increasing degree of hydroxylation, ultimately reaching the value of Cloisite 30B in the (PIOH-100)/Cloisite 30B

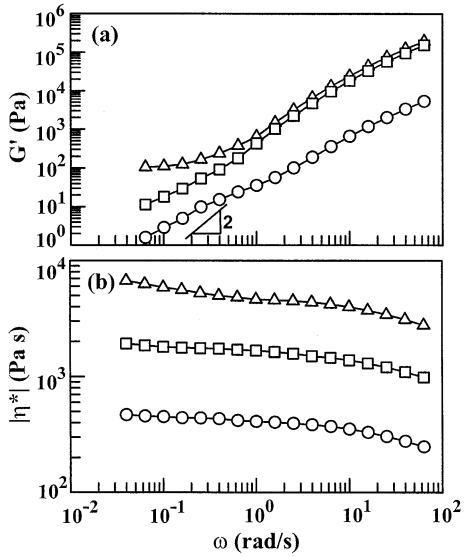

Figure 8. Plots of (a) log G' vs log ω and (b) log $|\eta^*|$ vs log ω at 180 °C for (○) EVAOH-5, (△) (EVAOH-5)/Cloisite 30B nanocomposite, and (□) (EVAOH-5)/Cloisite 15A nanocomposite.

nanocomposite. We now understand the reason why the (EVOH-53)/Cloisite 30B nanocomposite has such a poor degree of dispersion of Cloisite 30B aggregates (see Figure 4). The above observation was the basis upon which in this study we prepared partially hydrolyzed EVAOH-5 to prepare (EVAOH-5)/Cloisite 30B and (EVAOH-5)/Cloisite 15A nanocomposites.

Figure 8 gives (a) log G' vs log ω plots and (b) log $|\eta^*|$ vs log ω plots at 180 °C for EVAOH-5, (EVAOH-5)/Cloisite 30B, and (EVAOH-5)/Cloisite 15A. The following observations are worth noting in Figure 8. (i) Referring to Figure 8a, in the low-frequency region (ω < ca. 0.1 rad/s) of log G' vs log ω plots, the (EVAOH-5)/Cloisite 30B nanocomposite exhibits solidlike behavior, while the (EVAOH-5)/Cloisite 15A nanocomposite does not. Since the concentration of organoclay in the respective nanocomposites is the same (5 wt %), the observed difference in the rheological response in the terminal region of log G' vs log ω plots must be ascribed to the difference in the attractive interactions between EVAOH-5 and Cloisite 30B and between EVAOH-5 and Cloisite 15A. Since Cloisite 30B was treated with a surfactant MT2EtOH having hydroxyl groups while Cloisite 15A was treated with a surfactant 2M2HT that does not have any polar group, we attribute the observed difference in the rheological response between the (EVAOH-5)/Cloisite 30B and (EVAOH-5)/Cloisite 15A nanocomposites to an enhanced compatibility, via hydrogen bonding, between the hydroxyl groups in EVAOH-5 and the hydroxyl groups in the surfactant MT2EtOH residing at the surface of Cloisite 30B. Later in this paper we will present evidence, via in-situ FTIR spectroscopy, of the existence of hydrogen bonds in the (EVAOH-5)/Cloisite 30B over the entire range of experimental temperatures employed. (ii) In Figure 8b we observe that the $|\eta^*|$ of (EVAOH-5)/Cloisite 30B nanocomposite is about 10 times greater and the $|\eta^*|$ of (EVAOH-5)/Cloisite 15A nanocomposite is about 4 times greater than that of neat EVAOH-5. Since the concentration of organoclay in the respective nanocomposites is the same (5 wt %), the larger increase in $|\eta^*|$ for the (EVAOH-5)/Cloisite 30B nanocomposite is attributable to the presence of attractive interactions, via hydrogen

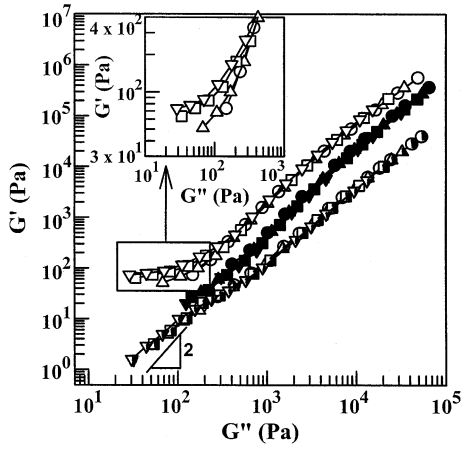

Figure 9. Plots of log G' vs log G'' for EVAOH-5 at 120 (◑), 140 (▲), 160 (◨), and 180 °C (▼); (EVAOH-5)/Cloisite 15A nanocomposite at 120 (●), 140 (▲), 160 (■), and 180 °C (▼); and (EVAOH-5)/Cloisite 30B nanocomposite at 120 (○), 140 (△), 160 (□), and 180 °C (▽).

bonding, between the hydroxyl groups in EVAOH-5 and the hydroxyl groups in the surfactant MT2EtOH.

Figure 9 gives log G' vs log G'' plots at 120, 140, 160, and 180 °C for EVAOH-5, (EVAOH-5)/Cloisite 30B, and (EVAOH-5)/Cloisite 15A nanocomposites. The following observations are worth noting in Figure 9. (i) The log G' vs log G'' plots for neat EVAOH-5 are independent of temperature, but their slopes in the terminal region are slightly less than 2. This observation is not surprising in that EVAOH-5 is a terpolymer having random distributions of ethylene, vinyl acetate, and vinyl alcohol, giving rise to a very broad molecular weight distribution. It has been pointed out earlier[49] that the slope of log G' vs log G'' plots for polydisperse polymers is expected to be 2 *only if* the applied frequency is sufficiently low (say much lower than 0.01 rad/s applied in the present study). (ii) The log G' vs log G'' plots for the (EVAOH-5)/Cloisite 15A nanocomposite are virtually independent of temperature over the range from 120 to 180 °C and have a slope slightly less than 2. This observations suggests that little change in morphology occurred in the (EVAOH-5)/Cloisite 15A nanocomposite as the temperature increased from 120 to 180 °C. Again, this is not surprising since little or no attractive interactions exist between EVAOH-5 and Cloisite 15A. (iii) We observe that at $G'' \geq 100$ Pa the log G' vs log G'' plots of (EVAOH-5)/Cloisite 30B nanocomposite are shifted upward by about 1 order of magnitude from those of neat EVAOH-5, and at G'' < 100 Pa the log G' vs log G'' plots of (EVAOH-5)/Cloisite 30B nanocomposite have a very small slope, exhibiting solidlike behavior. Most interestingly, a magnification of the log G' vs log G'' plots of (EVAOH-5)/Cloisite 30B nanocomposite at G'' < 100 Pa, shown in the inset of Figure 9, reveals a tendency that log G' vs log G'' plots are shifted upward as the temperature is increased from 120 to 180 °C. Such a temperature dependence of linear dynamic viscoelastic properties has never been observed in ordinary linear polymers. As a matter of fact, the temperature dependence of log G' vs log G'' plots observed in Figure 9 for the (EVAOH-5)/Cloisite 30B nanocomposite at G'' < 100 Pa is very similar to that observed in our previous studies, which investigated linear dynamic viscoelasticity of the nanocomposites composed of a polystyrene-*block*-hydroxylated polyisoprene copolymer and Cloisite 30B[12] and the nanocom-

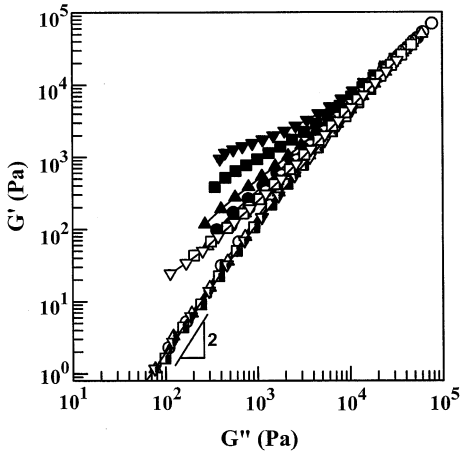

Figure 10. Plots of log G' vs log G'' for EVA at 120 (◑), 140 (▲), 160 (◨), and (▼) 180 °C; EVA/Cloisite 15A nanocomposite at 120 (●), 140 (▲), 160 (■), and (▼) 180 °C; and EVA/Cloisite 30B nanocomposite at 120 (○), 140 (△),160 (□), and (▽) 180 °C.

posites composed of polycarbonate (PC) and Cloisite 30B.[13]

We attribute the observed upward shift in the log G' vs log G'' plots of the (EVAOH-5)/Cloisite 30B nanocomposite, although its magnitude is small compared to that observed in our previous studies,[12,13] to an increase in the surface area that resulted from an enhanced dispersion of Cloisite 30B aggregates as the temperature increased from 120 to 180 °C. Later in this paper we will elaborate on this further. Comparison of Figure 9 with Figure 6 reveals clearly the difference in the temperature dependence of log G' vs log G'' plots between the (EVAOH-5)/Cloisite 30B and (EVOH-53)/Cloisite 30B nanocomposites. This observation now explains why the (EVAOH-5)/Cloisite 30B nanocomposite has a higher degree of dispersion of Cloisite 30B aggregates than the (EVOH-53)/Cloisite 30B nanocomposite (see Figure 4).

Figure 10 gives log G' vs log G'' plots at 120, 140, 160, and 180 °C for EVA, EVA/Cloisite 30B, and EVA/Cloisite 15A nanocomposites. The following observations are worth noting in Figure 10. (i) The log G' vs log G'' plots for EVA are virtually independent of temperature and have a slope very close to 2 in the terminal region, as is expected for all ordinary linear polymers with relatively narrow molecular weight distribution. (ii) The log G' vs log G'' plots for EVA/Cloisite 30B nanocomposite are also virtually independent of temperature but have a slope less than 2 in the terminal region, which is attributable to a "filler effect". The observation made above that the log G' vs log G'' plots for the EVA/Cloisite 30B nanocomposite are independent of temperature suggests to us that little change in morphology occurred in the nanocomposite as the temperature increased from 120 to 180 °C. This observation is not surprising since little or no attractive interactions are expected between the EVA and surfactant MT2EtOH. (iii) The log G' vs log G'' plots of EVA/Cloisite 15A nanocomposite is shifted upward as the temperature increases from 120 to 180 °C, indicating that the morphology of the nanocomposite changed with increasing temperature. We speculate that an increase in G' with increasing temperatures occurred because the surface areas of layered silicates increased with increasing temperature and that the increase in the surface area of layered silicates was realized by an enhanced dispersion (or exfoliation) of Cloisite 15A aggregates as temperatures increased from 120 to 180 °C. We repeated the experiments and obtained essentially the same results as presented in Figure 10.

After the rheological measurements, the nanocomposite specimens were quenched, and then XRD and TEM experiments were conducted, to determine whether the d_{001} spacing and the degree of exfoliation of the organoclay, which had been attained during the oscillatory shear flow experiment, was preserved or not after the quenching. We obtained from the XRD patterns virtually the same value of d_{001} spacing of the organoclay before and after the oscillatory shear flow experiments. Also, we were not able to discern from the TEM images any differences in the degree of exfoliation of the specimens before and after the oscillatory shear flow experiments. The primary reason for such experimental findings was that the nanocomposites were prepared by melt blending using a Brabender mixer, resulting in a nonuniform spatial distribution of the organoclay aggregates in the polymer matrix, which was essentially averaged out over very limited and specific areas chosen in the XRD and TEM experiments.

The temperature dependence of log G' vs log G'' plots shown in Figure 10 for the EVA/Cloisite 15A nanocomposite points out that time−temperature superposition (TTS) *fails* for the nanocomposite. A question remains to be answered as to why the temperature dependence of log G' vs log G'' plots for the EVA/Cloisite 15A nanocomposite is so different from that for the EVA/Cloisite 30B nanocomposite. Later in this paper we will answer this question.

An upward shift in the log G' vs log G'' plots of EVA/Cloisite 15A nanocomposite, observed in Figure 10, cannot be ascribed to thermal degradation of EVA and/or the decomposition gases from the surfactant 2M2HT residing at the surface of Cloisite 15A. If chain degradation of EVA had been extensive, we should have observed a decrease of G' in the EVA/Cloisite 15A nanocomposite as the temperature increased because the smaller the size of macromolecules, the lower will be the values of G'. Another possibility that could have caused the increased values of G' of the EVA/Cloisite 5A nanocomposite with increasing temperature might be cross-linking reactions of EVA molecule themselves or chemical reactions between EVA and 2M2HT. We cannot find any plausible mechanisms for the cross-linking reactions of EVA molecule themselves or chemical reactions between EVA and 2M2HT, which could take place at temperatures ranging from 120 to 180 °C. Since the aliphatic chains in the tallow of surfactant 2M2HT are saturated, little or no chance exists for the hydrogenated tallow to have undergone cross-linking reactions. Even if we were to suppose that the hydrogenated aliphatic chains in the tallow of 2M2HT decomposed at temperatures between 120 and 180 °C, although this is highly unlikely, the amount of hydrogenated aliphatic chains of the tallow are so small (estimated to be less than 0.5 wt % in the EVA/Cloisite 15A nanocomposite) that they could not possibly have increased the values of G' of the EVA/Cloisite 15A nanocomposite 1 order of magnitude as the temperature increased from 120 to 180 °C (see Figure 10).

Figure 11 gives log $|\eta^*|$ vs log ω plots at 120, 140, 160, and 180 °C for EVA, EVA/Cloisite 30B, and EVA/Cloisite 15A nanocomposites. The following observations are

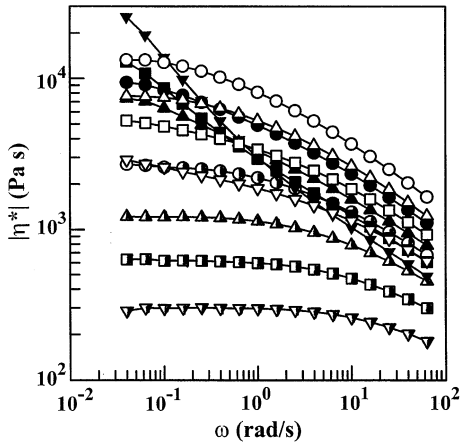

Figure 11. Plots of log $|\eta^*|$ vs log ω for EVA at 120 (◑), 140 (▲), 160 (◨), and (▼) 180 °C; EVA/Cloisite 15A nanocomposite at 120 (●), 140 (▲), 160 (■), and (▼) 180 °C; and EVA/Cloisite 30B nanocomposite at 120 (○), 140 (△),160 (□), and (▽) 180 °C.

worth noting in Figure 11. (i) The log $|\eta^*|$ vs log ω plots for EVA exhibit Newtonian behavior, and values of $|\eta^*|$ decrease with increasing temperature, as is expected for all ordinary linear polymers. (ii) The log $|\eta^*|$ vs log ω plots for EVA/Cloisite 30B nanocomposite show very weak shear-thinning behavior in the low-frequency region, suggesting that little attractive intermolecular interactions exist between the EVA molecules and surfactant MT2EtOH residing at the surface of Cloisite 30B. Note that values of $|\eta^*|$ for EVA/Cloisite 30B nanocomposite are larger than those of neat EVA, and they decrease with increasing temperature. (iii) In the low-frequency region, the log $|\eta^*|$ vs log ω plots of EVA/Cloisite 15A nanocomposite exhibit shear-thinning behavior over the entire range of angular frequencies and at all four temperatures tested. Notice that at $\omega <$ ca. 0.1 rad/s the $|\eta^*|$ of EVA/Cloisite 15A nanocomposite increased as the temperature increased from 140 to 180 °C, at which a very strong shear-thinning behavior is observed. At $\omega = 0.1$ rad/s the $|\eta^*|$ of EVA/Cloisite 15A nanocomposite at 180 °C is about 2 orders of magnitude greater than that of neat EVA. Such a large increase in $|\eta^*|$ at 180 °C is attributable to an increase in the surface area of layered silicates with increasing temperature, which is only possible when organoclay aggregates are highly exfoliated with increasing temperature. After all, the very unusual temperature dependence of complex viscosity for the EVA/Cloisite 15A nanocomposite presented in Figure 11 is not surprising because this observation is consistent with that made above in reference to Figure 10. Again, the experiments were repeated, and essentially the same results as presented in Figure 11 were obtained.

Transient and Intermittent Shear Flows of Organoclay Nanocomposites Based on EVOH or EVAOH. In the present study we conducted transient shear flow and, also, intermittent shear flow with a rest for a predetermined period after cessation of the initial transient for EVOH/organoclay and EVAOH/organoclay nanocomposites. For the experiments, a specimen was subjected to a sudden shear flow (often referred to as start-up of shear flow or initial transient shear flow) at a predetermined shear rate ($\dot{\gamma}$) and 180 °C. After the initial transient shear flow reached steady state, the flow was stopped and the specimen was at rest for a predetermined period (5, 20, 40, or 60 min). Then the same specimen was subjected to another sudden shear flow (often referred to as intermittent shear flow or interrupted shear flow) until reaching steady state. During the entire period of initial transient and intermittent shear flows, variations of shear stress growth ($\sigma^+(\dot{\gamma},t)$) and first normal stress growth ($N_1^+(\dot{\gamma},t)$) were monitored.

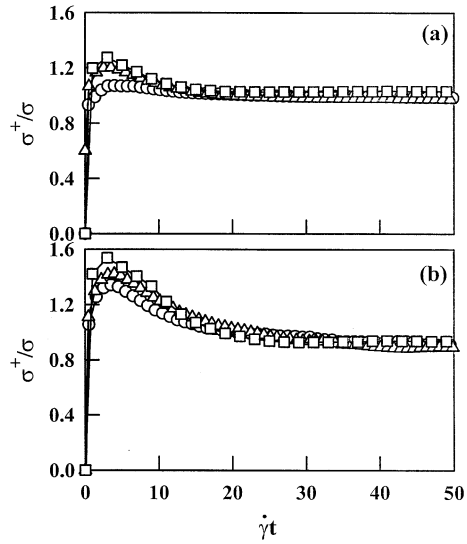

Figure 12. Variations of $\sigma^+(\dot{\gamma},t)/\sigma$ with $\dot{\gamma}t$ at 180 °C during start-up of shear flow of (a) EVAOH-5 and (b) (EVAOH-5)/Cloisite 30B nanocomposite at different shear rates: (○) $\dot{\gamma} = 0.5$ s^{-1}; (△) $\dot{\gamma} = 1.0$ s^{-1}; (□) $\dot{\gamma} = 2.0$ s^{-1}.

Figure 12 describes the evolution of normalized shear stress growth, $\sigma^+(\dot{\gamma},t)/\sigma$, upon start-up of shear flow, with the applied shear strain ($\dot{\gamma}t$) for (a) EVAOH-5 and (b) (EVAOH-5)/Cloisite 30B nanocomposite at 180 °C for three different values of shear rate ($\dot{\gamma}$): 0.5, 1.0, and 2.0 s^{-1}, in which σ is steady-state shear stress. In Figure 12 we observe that (i) an overshoot peak σ_{peak}^+ in EVAOH-5 appears and then levels off, reaching steady state, and the value of σ_{peak}^+ increases with increasing $\dot{\gamma}$; (ii) the values of σ_{peak}^+ for the (EVAOH-5)/Cloisite 30B nanocomposite are much larger than those for EVAOH-5, signifying that attractive interactions exist between EVAOH-5 and Cloisite 30B; (iii) strain scaling holds for the nanocomposite transient data. Previously, Solomon et al.[57] reported on successful strain scaling of transient shear data for polypropylene/organoclay nanocomposites. According to Larson,[58] the idea behind the use of strain scaling is that a microstructural relaxation time τ is manipulated by the applied strain with a form $\tau \sim \dot{\gamma}^{-1}$. Thus, scaling shearing time by relaxation time suggests superposition of data at varying shear rates as t/τ or $\dot{\gamma}t$.

Figure 13 describes the evolution of normalized first normal stress difference growth, $N_1^+(\dot{\gamma},t)/N_1$, upon start-up of shear flow, with the applied $\dot{\gamma}t$ for (EVAOH-5)/Cloisite 30B nanocomposite at 180 °C for three different values of $\dot{\gamma}$: 0.5, 1.0, and 2.0 s^{-1}, where N_1 is steady-state first normal stress difference. In Figure 13 we observe very irregular behavior of $N_1^+(\dot{\gamma},t)/N_1$ over the entire range of applied $\dot{\gamma}t$, and there is absolutely no strain scaling. Most importantly, we were not able to obtain reproducible $N_1^+(\dot{\gamma},t)$ data for the (EVAOH-5)/Cloisite 30B nanocomposite and also for other nanocomposites, although they are not presented here. It is then clear why so little has been reported on transient first normal stress difference for organoclay nanocomposites.

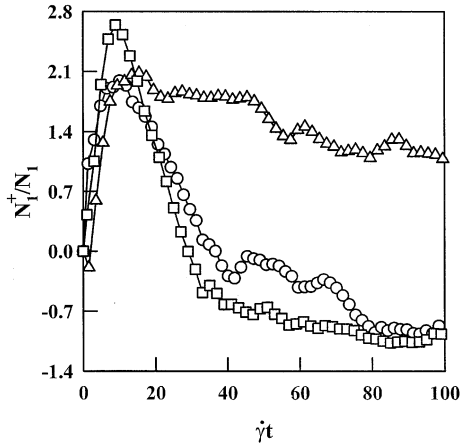

Figure 13. Variations of $N_1^+(\dot{\gamma},t)/N_1$ with $\dot{\gamma}t$ at 180 °C during start-up of shear flow for (EVAOH-5)/Cloisite 30B nanocomposite at different shear rates: (○) $\dot{\gamma} = 0.5\ s^{-1}$; (△) $\dot{\gamma} = 1.0\ s^{-1}$; (□) $\dot{\gamma} = 2.0\ s^{-1}$.

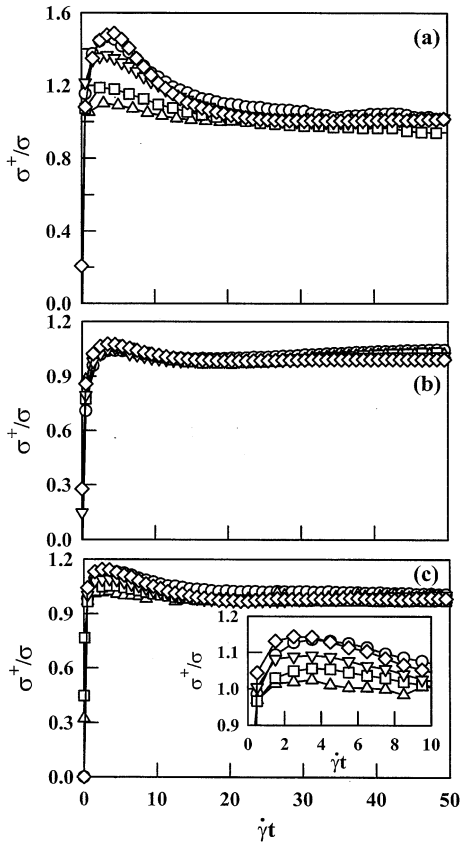

Figure 14. Variations of $\sigma^+(\dot{\gamma},t)/\sigma$ with $\dot{\gamma}t$ at 180 °C during transient/intermittent shear flows at $\dot{\gamma} = 1.0\ s^{-1}$ for (a) (EVAOH-5)/Cloisite 30B nanocomposite during the initial transient shear flow (○) and intermittent shear flow after rest for different periods: (△) 5 , (□) 20 , (▽) 40 , and (◇) 60 min; (b) (EVOH-53)/Cloisite 30B nanocomposite during the initial transient shear flow (○) and intermittent shear flow after rest for different periods: (△) 5 , (□) 20 , (▽) 40, and (◇) 60 min; (c) (EVAOH-5)/Cloisite 15A nanocomposite during the initial transient shear flow (○) and intermittent shear flow after rest for different periods: (△) 5 , (□) 20, (▽) 40, and (◇) 60 min.

Figure 14 describes the evolution of $\sigma^+(\dot{\gamma},t)/\sigma$ with the applied $\dot{\gamma}t$ for (a) (EVAOH-5)/Cloisite 30B nanocomposite, (b) (EVOH-53)/Cloisite 30B nanocomposite, and (c) (EVAOH-5)/Cloisite 15A nanocomposite during the initial transient shear flow (○) and during the intermittent shear flow after a rest for 5 (△), 20 (□), 40 (▽), and 60 min (◇). The reason for having performed such experiments was to determine whether the morphology of the nanocomposites evolves with time during a rest upon cessation of the initial transient shear flow. The following observations are worth noting in Figure 14.

Referring to Figure 14a, a large overshoot peak σ_{peak}^+ for the (EVAOH-5)/Cloisite 30B nanocomposite appears in the initial transient (○), but the value of σ_{peak}^+ during intermittent shear flow after a rest for 5 min (△) is very small. Interestingly, the value of σ_{peak}^+ during intermittent shear flow gradually increases as the period of rest upon cessation of the initial transient increases to 20 min (□) and then to 40 min (▽), and after a rest for 60 min (◇) it finally overlaps with the value of σ_{peak}^+ (○) in the initial transient. This observation suggests that reorganization of structure in the (EVAOH-5)/Cloisite 30B nanocomposite took place during a rest upon cessation of shear flow, which is only possible when attractive interactions exist between the hydroxyl groups in EVAOH and the hydroxyl groups in the surfactant MT2EtOH residing at the surface of Cloisite 30B. Supporting evidence of this observation can be found in Figure 14b for the (EVOH-53)/Cloisite 30B nanocomposite, showing that the value of σ_{peak}^+ remains constant regardless of the period of rest upon cessation of shear flow and the magnitude of σ_{peak}^+ for this nanocomposite is much smaller compared to that for the (EVAOH-5)/Cloisite 30B nanocomposite (see Figure 14a). The intermittent shear flow behavior of the (EVOH-53)/Cloisite 30B nanocomposite given in Figure 14b suggests that no reorganization of structure took place during a rest upon cessation of shear flow. This is because *no* attractive interactions exist between the hydroxyl groups in EVOH-53 and the hydroxyl groups in the surfactant MT2EtOH, as was already discussed when presenting XRD patterns in Figure 3 and TEM images in Figure 4.

Referring to Figure 14c for the (EVAOH-5)/Cloisite 15A nanocomposite, we observe that the magnitude of overshoot peak σ_{peak}^+ is much smaller than that for the (EVAOH-5)/Cloisite 30B nanocomposite (see Figure 14a) and the value of σ_{peak}^+ shows a very weak dependence of the rest period upon cessation of shear flow. That is, the intermittent shear flow behavior of the (EVAOH-5)/Cloisite 15A nanocomposite lies between that of the (EVAOH-5)/Cloisite 30B nanocomposite and the (EVOH-53)/Cloisite 30B nanocomposite. This observation is consistent with that made from XRD patterns (see Figure 3) and TEM images (see Figure 4) in that (i) the d_{001} spacing of the (EVAOH-5)/Cloisite 15A nanocomposite is slightly larger than that of the (EVOH-53)/Cloisite 30B nanocomposite but much smaller than that of the (EVAOH-5)/Cloisite 30B nanocomposite, and (ii) the degree of dispersion of organoclay aggregates is higher in the (EVAOH-5)/Cloisite 15A composite than in the (EVOH-53)/Cloisite 30B nanocomposite but not as good as in the (EVAOH-5)/Cloisite 30B nanocomposite.

Figure 15 describes the evolution of $\sigma^+(\dot{\gamma},t)/\sigma$ with the applied $\dot{\gamma}t$ for (a) EVA/Cloisite 15A nanocomposite and (b) EVA/Cloisite 30B nanocomposite during the initial transient shear flow (○) and during the intermittent shear flow after a rest for 5 (△), 20 (□), 40 (▽), and 60 min (◇). Referring to Figure 15a, a large overshoot peak σ_{peak}^+ for the EVA/Cloisite 15A nanocomposite appears in the initial transient (○), but the value of σ_{peak}^+ during intermittent shear flow after a rest for 5 min (△) is very

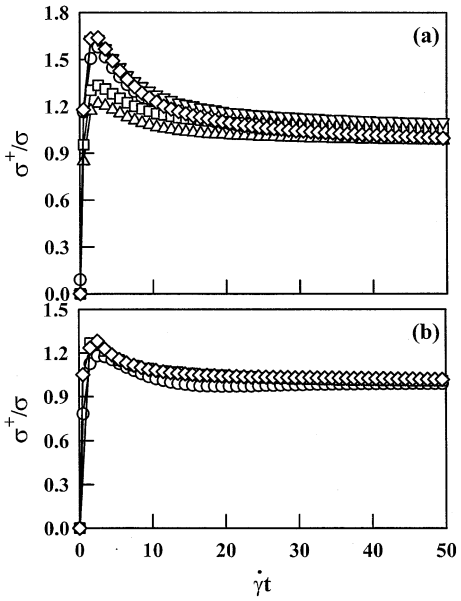

Figure 15. Variations of $\sigma^+(\dot{\gamma},t)/\sigma$ with $\dot{\gamma}t$ at 180 °C during transient/intermittent shear flows at $\dot{\gamma} = 1.0\ s^{-1}$ for (a) EVA/Cloisite 15A nanocomposite during the initial transient shear flow (○) and intermittent shear flow after rest for different periods: (△) 5 , (□) 20, (▽) 40, and (◇) 60 min; (b) EVA/Cloisite 30B nanocomposite during the initial transient shear flow (○) and intermittent shear flow after rest for different periods: (△) 5 , (□) 20 , (▽) 40 , and (◇) 60 min.

small, but it gradually increases as the period of rest upon cessation of the initial transient increases to 20 min (□) and then to 40 min (▽), and finally it overlaps with that of the initial transient after a rest for 60 min (◇). This observation is very similar to that made above for the (EVAOH-5)/Cloisite 30B nanocomposite given in Figure 14a.

Referring to Figure 15b, we observe that the value of $\sigma_{peak}{}^+$ for the EVA/Cloisite 30B nanocomposite remains constant regardless of the period of rest upon cessation of shear flow, very similar to the observation made above for the (EVOH-53)/Cloisite 30B nanocomposite given in Figure 14b. Thus, we conclude from Figure 15b that no or little attractive interactions exist between EVA and Cloisite 30B. This observation is consistent with the results from the XRD patterns given in Figure 3 in that the d_{001} spacing of the EVA/Cloisite 30B nanocomposite is only slightly larger than that of Cloisite 30B and from the TEM images given in Figure 4 in that the degree of dispersion of organoclay aggregates in the EVA/Cloisite 30B nanocomposite is very poor compared to that in the EVA/Cloisite 15A nanocomposite.

4. Discussion

Origins of the Differences in the Degree of Exfoliation and the Temperature Dependence of Linear Dynamic Viscoelasticity between (EVAOH-5)/Cloisite 30B and (EVAOH-5)/Cloisite 15A Nanocomposites. Figure 16 gives in-situ FTIR spectra of (a) (EVAOH-5)/Cloisite 30B and (b) (EVAOH-5)/Cloisite 15A at temperatures ranging from 25 to 180 °C. In Figure 16a, the absorption band for the hydrogen-bonded hydroxyl groups appears at ca. 3330 cm^{-1}, and the area under the absorption band at ca. 3330 cm^{-1} for the (EVAOH-5)/Cloisite 30B nanocomposite decreases very slowly as the temperature is increased from 25 to 180 °C. The absorption band at ca. 3330 cm^{-1} still

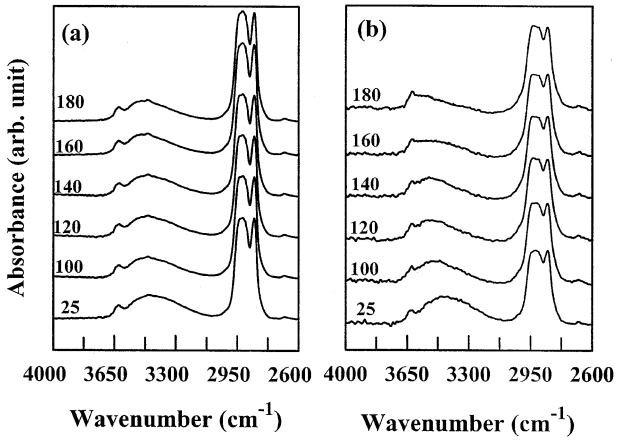

Figure 16. In-situ FTIR spectra for (a) (EVAOH-5)/Cloisite 30B nanocomposite and (b) (EVAOH-5)/Cloisite 15A nanocomposite.

persists at 180 °C, the highest experimental temperature employed. On the other hand, it is seen from Figure 16b that the area under the absorption band at ca. 3330 cm^{-1} for the (EVAOH-5)/Cloisite 15A nanocomposite decreases gradually with increasing temperature and disappears completely at 180 °C. Since there is no polar group in the surfactant 2M2HT residing at the surface of organoclay Cloisite 15A, it is very reasonable to conclude that the steady decrease in the area under the absorption band at ca. 3330 cm^{-1} for the (EVAOH-5)/Cloisite 15A nanocomposite (Figure 16b) signifies the gradual weakening of the *intramolecular* forces (due to the presence of hydroxyl groups) within EVAOH-5 molecules themselves. It is well established that the strength of hydrogen bonds in a polymer decreases with increasing temperature.[14] This observation then leads us to conclude that the persistence of the absorption band at ca. 3330 cm^{-1} up to 180 °C (Figure 16a) is due to the presence of attractive interactions (hydrogen bonding) between the hydroxyl groups in EVAOH-5 and the hydroxyl groups in the surfactant MT2EtOH residing at the surface of organoclay Cloisite 30B.

We attempted to determine the percentage of hydrogen-bonding sites on the Cloisite 30B surface by deconvoluting the overlapping peaks in the FTIR spectra shown in Figure 16, but found this to be a very difficult task, if not impossible, since the amount of the hydroxyl groups associated with the organoclay Cloisite 30B in the nanocomposite was so small (estimated to be less than 0.2%). What made the situation worse was that an accurate determination, via ^1H nuclear magnetic resonance (NMR) spectroscopy, of the amount of the hydroxyl groups in the surfactant MT2EtOH was found to be extremely difficult due to the very complex nature of its chemical structure.

On the basis of Figure 16, we conclude that the very broad, indistinguishable intensity peak observed from XRD patterns (Figure 3), the relatively high degree of exfoliation observed from TEM images (Figure 4), and very unusual temperature dependence of log G' vs log G'' plots observed from oscillatory shear flow experiments (Figure 9) in the (EVAOH-5)/Cloisite 30B nanocomposite have originated from the presence of strong attractive interactions, via hydrogen bonding, between the hydroxyl groups in EVAOH-5 and the hydroxyl groups in the surfactant MT2EtOH residing at the surface of Cloisite 30B.

There is another factor, the gallery distance of organoclay itself, which can affect the degree of exfoliation of organoclay aggregates. The gallery distance of an organoclay depends on the chemical structure of a surfactant that is applied to the surface of the aggregates of pristine montmorillonite. It is shown in Figure 3 that the d_{001} spacing of Cloisite 30B is 1.85 nm and the d_{001} spacing of Cloisite 15A is 3.15 nm. On the basis of the difference in the gallery distance between the two organoclays, it is reasonable to expect that the (EVAOH-5)/Cloisite 15A nanocomposite would have a higher degree of exfoliation than the (EVAOH-5)/Cloisite 30B nanocomposite. However, the experimental results (Figure 4) stand in contrast with the expectation. Note in Figure 16 that the compatibility between EVAOH-5 and Cloisite 30B is much greater owing to the presence of hydrogen bonding than the compatibility between EVAOH-5 and Cloisite 15A. The above observation seems to suggest that the compatibility between polymer matrix and organoclay plays a predominant role over the difference in the gallery distance of two organoclays in determining the degree of exfoliation of organoclay aggregates. This is quite understandable in that when strong repulsive forces exist between polymer matrix and organoclay (i.e., when the two are incompatible), the polymer molecules will not be able to approach the surface of the layered silicates and thus be unable to exfoliate organoclay aggregates or peel away the top and bottom layers as promoted by the polymer adsorption and the application of shear stress.

Origins of the Differences in the Degree of Exfoliation and the Temperature Dependence of Linear Dynamic Viscoelasticity between EVA/Cloisite 15A and EVA/Cloisite 30B Nanocomposites. We have shown that the EVA/Cloisite 15A nanocomposite has a larger d_{001} spacing (Figure 3) and a higher degree of exfoliation (Figure 4) than the EVA/Cloisite 30B nanocomposite, and the log G' vs log G'' plot of the EVA/Cloisite 15A nanocomposite is shifted upward with increasing temperature, while the log G' vs log G'' plot of the EVA/Cloisite 30B nanocomposite is independent of temperature (Figure 8). The above experimental observations suggest that the compatibility between EVA and Cloisite 15A is better than the compatibility between EVA and Cloisite 30B, granted that the d_{001} spacing (3.15 nm) of Cloisite 15A is much larger than d_{001} spacing (1.85 nm) of Cloisite 30B. Referring to Figure 9, we already have pointed out that an organoclay having a larger d_{001} spacing will help in the dispersion (or exfoliation) of organoclay aggregates *only when* attractive interactions exist between the organoclay and polymer matrix.

In the present study we made an attempt to generate experimental evidence, indicating that the compatibility between EVA and Cloisite 15A is greater than that between EVA and Cloisite 30B. For this, we took the following simplified approach, namely, we investigated the phase behavior, via cloud point measurements, between pol(vinyl acetate) (PVAc) and surfactant 2M2HT and between PVAc and surfactant MT2EtOH. The rationale behind this approach lies in the stipulation that the ethylene in EVA would not be miscible with 2M2HT or MT2EtOH. Thus, the problem has been much simplified by focusing on the miscibility between PVAc (instead of random copolymer EVA) and surfactant 2M2HT or surfactant MT2EtOH. For this purpose we purchased a low-molecular-weight PVAc (Aldrich) having a weight-average molecular weight of 1.85×10^4 g/mol. Then we prepared binary mixtures of PVAc, via solution blending in chloroform, with 2M2HT or MT2EtOH having various compositions ranging from 10 to 90 wt % and conducted cloud point measurements using laser light scattering.

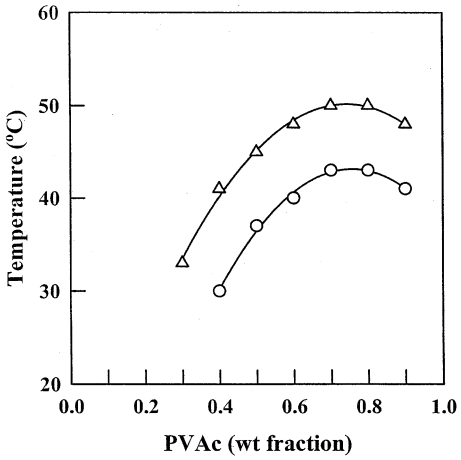

Figure 17. Binodal curves for: (○) PVAc/2M2HT mixtures and (△) PVAc/MT2EtOH mixtures.

Figure 17 gives binodal curves for PVAc/2M2HT mixtures (○) and PVAc/MT2EtOH mixtures (△), showing upper critical solution temperature (USCT) behavior. It is interesting to observe in Figure 17 that the PVAc/2M2HT pair has a lower UCST than the PVAc/MT2EtOH pair, suggesting that the miscibility of PVAc/2M2HT pair is better than the miscibility of PVAc/MT2EtOH pair. The above experimental results, although very crude, seem to explain why the compatibility between EVA and Cloisite 15A is better than the compatibility between EVA and Cloisite 30B, as evidenced by TEM images (Figure 4), the temperature dependence of log G' vs log G'' plots (Figure 9), and nonlinear transient rheology (Figure 15). We are well aware of the fact that in the EVA/Cloisite 15A and EVA/Cloisite 30B nanocomposites there would be little chance for direct contact between the vinyl acetate molecules in EVA and surfactant 2M2HT or MT2EtOH residing at the surface of organoclay (Cloisite 15A or Cloisite 30B) and that vinyl acetate and ethylene molecules are randomly distributed in a EVA chain. There are two reasons why we chose PVAc, instead of EVA, to obtain binodal curves using cloud point measurements. One reason was that we needed a low-molecular-weight EVA to prepare binary mixtures with surfactant 2M2HT or MT2EtOH because the surfactants were organic substances having very low molecular weights; however, low-molecular-weight EVA was not available to us. Another reason was that even if a low-molecular-weight EVA had been available to us, we would not have been able to find a common solvent that dissolves both EVA and surfactant 2M2HT or MT2EtOH. Although the approach taken in this study was very crude, the cloud point measurements summarized in Figure 17 help us to explain, at least qualitatively, why the EVA/Cloisite 15A nanocomposite has a higher degree of exfoliation of organoclay aggregates (Figure 4) than the EVA/Cloisite 30B nanocomposite and why the log G' vs log G'' plot of EVA/Cloisite 15A nanocomposite is shifted upward with increasing temperature while the log G' vs log G'' plot of EVA/Cloisite 30B

nanocomposite is virtually independent of temperature (Figure 10). For the EVA/Cloisite 15A nanocomposite, we believe that the larger gallery distance of Cloisite 15A, in the presence of attractive interactions between EVA and Cloisite 15A, must have played an important role in increasing the degree of exfoliation of Cloisite 15A aggregates.

There are two additional factors that contributed to the upward shift in the log G' vs log G'' plot with increasing temperature for the EVA/Cloisite 15A nanocomposite (see Figure 10). They are an increase in the surface area of layered silicates and a decrease in the melt viscosity of EVA as the temperature increased from 120 to 180 °C. An increase in the surface area of layered organoclay platelets will occur when polymer matrix and organoclay are compatible, enhancing the dispersion of organoclay aggregates. The larger the surface area of organoclay platelets, the greater will be the values of G' and G'' during small-amplitude oscillatory shear flow. It is well-established today that the dynamic storage modulus G' is much more sensitive than the dynamic loss modulus G'' to variations in morphology during small-amplitude oscillatory shear flow. It is estimated that the melt viscosity of EVA decreases more than 1 order of magnitude as the temperature is increased from 120 to 180 °C. Thus, the mobility of EVA molecules in the nanocomposite must have been increased dramatically as the temperature increased from 120 to 180 °C. In turn, the markedly enhanced mobility of EVA molecules must have helped increase the degree of dispersion (or exfoliation) of Cloisite 15A aggregates in the EVA/Cloisite 15A nanocomposite as the temperature increased from 120 to 180 °C, giving rise to vastly increased surface area of Cloisite 15A platelets. Needless to state, a decrease in the viscosity of EVA with increasing temperatures would *not* have helped increase the degree of exfoliation of Cloisite 15A aggregates *if* EVA and Cloisite 15A had not been compatible.

5. Concluding Remarks

In this study, we investigated the rheological behavior of six organoclay nanocomposites based on EVA, EVOH-53, and EVAOH-5. For the study we employed two organoclays: Cloisite 30B with a surfactant MT2EtOH having hydroxyl groups and Cloisite 15A with a surfactant having no hydroxyl group. We found significant differences in the degree of exfoliation of organoclay aggregates and rheological responses among the six nanocomposites investigated. The experimental results are interpreted in terms of the compatibility between polymer matrix and the surfactant residing at the surface of organoclay and the gallery distance of the organoclays. Specifically, we found *little* evidence of compatibility between EVOH-53 and surfactant MT2EtOH residing at the surface of Cloisite 30B. We have attributed this observation to the very strong *intramolecular* attractive forces within EVOH-53 molecule themselves, inhibiting *intermolecular* attractive interactions (hydrogen bonding) between the hydroxyl groups in EVOH-53 and the hydroxyl group in the surfactant MT2EtOH. On the other hand, we observed evidence, via in-situ FTIR spectroscopy, of the formation of hydrogen bonds between the hydroxyl groups in EVAOH-5 and the hydroxyl group in the surfactant MT2EtOH. The TEM images show that Cloisite 30B aggregates are reasonably well dispersed in the (EVAOH-5)/Cloisite 30B nanocomposite but poorly dispersed in the (EVOH-53)/Cloisite 30B nanocomposite. We found that the EVA/Cloisite 15A nanocomposite has a higher degree of exfoliation of organoclay aggregates than the EVA/Cloisite 30B nanocomposite. We also conducted cloud point measurements for mixtures of a low-molecular-weight poly(vinyl acetate) (PVAc) and surfactant 2M2HT or surfactant MT2EtOH to investigate the miscibility between PVAc and 2M2HT and between PVAc and MT2EtOH. We found that both mixtures exhibit UCST behavior, and the UCST of PVAc/2M2HT mixtures is lower than that of PVAc/MT2EtOH mixtures, indicating that the miscibility of PVAc/2M2HT mixtures is better than that of PVAc/MT2EtOH mixtures. We have used this experimental observation to explain why the EVA/Cloisite 15A nanocomposite has a higher degree of exfoliation of organoclay aggregates than the EVA/Cloisite 30B nanocomposite.

In the present study we have shown that the log G' vs log G'' plots of (EVAOH-5)/Cloisite 30B and EVA/Cloisite 15A nanocomposites are shifted upward, while the log G' vs log G'' plots of (EVAOH-5)/Cloisite 15A and EVA/Cloisite 30B nanocomposites remain constant, as the temperature is increased from 120 to 180 °C. We have attributed the observed upward shift in the log G' vs log G'' plots of (EVAOH-5)/Cloisite 30B and EVA/Cloisite 15A nanocomposites to an increase in the surface areas of organoclay platelets due to an enhanced compatibility between the polymer matrix and organoclay.

We have shown that the gallery distance of an organoclay may influence the degree of exfoliation of organoclay aggregates only when polymer matrix and organoclay are compatible. We have demonstrated this by showing that the (EVAOH-5)/Cloisite 30B nanocomposite has a much higher degree of dispersion of organoclay aggregates than the (EVAOH-5)/Cloisite 15A nanocomposite (see Figure 4), although Cloisite 15A has a larger gallery distance than Cloisite 30B. This is because the hydroxyl groups in EVAOH-5 and the hydroxyl groups in the surfactant MT2EtOH residing at the surface of Cloisite 30B formed hydrogen bonds, enhancing the compatibility between Cloisite 30B and EVAOH-5 (see Figure 16). On the other hand, little or no evidence of compatibility between Cloisite 15A and EVAOH-5 was found, giving rise to poor dispersion of Cloisite 15A aggregates in EVAOH-5.

We also have pointed out that melt viscosity of polymer matrix plays an important role in dispersing (or exfoliating) organoclay aggregates only when polymer matrix and organoclay are compatible. Since intercalation or exfoliation of organoclay aggregates requires the diffusion of polymer molecules into the galleries of layered silicates or peel away of the top and bottom layers as promoted by the polymer adsorption and the application of shear stress, the mobility of polymer matrix should play an important role in exfoliating organoclay aggregates.

We measured the tensile properties of the six nanocomposites prepared in this study, and the results are summarized in Table 4. We observe from Table 4 that, disappointingly to a certain extent, improvements in Young's modulus, maximum tensile stress, and present elongation of the nanocomposites over the neat polymers are very moderate. On the other hand, the purpose of preparing organoclay nanocomposites is not always to improve mechanical properties. Improvement in other physical properties, such as gas permeability, optical

Table 4. Tensile Properties of the Organoclay Nanocomposites Investigated in This Study

sample code	Young's modulus (MPa)	max tensile stress (MPa)	elongation (%)
EVA	1.2×10^1	39	2.0×10^3
EVA/Cloisite 30B	2.6×10^1	41	1.8×10^3
EVA/Cloisite 15A	2.8×10^1	43	1.7×10^3
EVAOH-5	1.0×10^2	93	1.4×10^3
(EVAOH-5)/Cloisite 30B	1.1×10^2	126	1.4×10^3
(EVAOH-5)/Cloisite 15A	1.1×10^2	112	1.3×10^3
EVOH-53	8.2×10^3	363	4.5×10^1
(EVOH-53)/Cloisite 30B	9.6×10^3	419	3.4×10^1
(EVOH-53)/Cloisite 15A	9.8×10^3	392	3.4×10^1

clarity, flammability, etc., can be realized by adding low volumes (1−5%) of highly anisotropic organoclays having very large aspect ratios. Improvement in such physical properties requires good dispersion (high degree of exfoliation) of organoclay in the polymer matrix.

Acknowledgment. We acknowledge with gratitude that Southern Clay Products provided us with the organoclays employed in this study. This study was supported in part by LG Chemical Ltd.

References and Notes

(1) LeBaron, R. C.; Wang, Z.; Pinnavaia, T. *J. Appl. Clay Sci.* **1999**, *15*, 11.
(2) Giannelis, E. P.; Krishnamoorti, R.; Manias, E. *Adv. Polym. Sci.* **1999**, *138*, 107.
(3) Kato, M.; Usuki, A. In *Polymer-Clay Nanocomposites*, Pinnavaia, T. J., Beall, G. W., Eds.; Wiley: New York, 2000; p 97.
(4) Komori, Y.; Kuroda, K. In *Polymer-Clay Nanocomposites*, Pinnavaia, T. J., Beall, G. W., Eds.; Wiley: New York, 2000; p 3.
(5) Sur, G. S.; Sun, H. L.; Lyu, S. G.; Mark, J. E. *Polymer* **2001**, *42*, 9783.
(6) Vaia, R. A.; Giannelis, E. P. *Macromolecules* **1997**, *30*, 7990.
(7) Vaia, R. A.; Giannelis, E. P. *Macromolecules* **1997**, *30*, 8000.
(8) Balazs, A. C.; Singh, C.; Zhulina, E. *Macromolecules* **1998**, *31*, 8370.
(9) Lyatskaya, Y.; Balazs, A. C. *Macromolecules* **1998**, *31*, 6676.
(10) Balazs, A. C.; Singh, C.; Zhulina, E.; Lyatskaya, Y. *Acc. Chem. Res.* **1999**, *32*, 651.
(11) Kuznetsov, V. D.; Balazs, C. A. *J. Chem. Phys.* **2000**, *112*, 4365.
(12) Lee, K. M.; Han, C. D. *Macromolecules* **2003**, *36*, 804.
(13) Lee, K. M.; Han, C. D. *Polymer* **2003**, *44*, 4573.
(14) Coleman, M. M.; Graf, J. F.; Painter, P. C. *Specific Interactions and the Miscibility of Polymer Blends*; Technomic: Lancaster, PA, 1991.
(15) Messersmith, P. B.; Giannelis, E. P. *Chem. Mater.* **1993**, *5*, 1064.
(16) Messersmith, P. B.; Giannelis, E. P. *J. Polym. Sci., Polym. Phys. Ed.* **1995**, *33*, 1047.
(17) Hoffmann. B.; Kressler, J.; Stöppelmann, G.; Fredrich, C.; Kim, G. M. *Colloid Polym. Sci.* **2000**, *278*, 629.
(18) Lepoittevin, B.; Pantoustier, N.; Devalckenaere, M.; Alexandre, M.; Kubies, D.; Calberg, D.; Jérôme, R.; Dubois, P. *Macromolecules* **2002**, *35*, 8385.
(19) Kato, M.; Usuki, A.; Okada, A. *J. Appl. Polym. Sci.* **1997**, *66*, 1781.
(20) Kawasu, M.; Hasegawa, N.; Kato, M.; Usuki, A.; Okada, A. *Macromolecules* **1997**, *30*, 6333.
(21) Hasegawa, N.; Kawasumi, M.; Kato, M.; Usuki, A.; Okada, A. *J. Appl. Polym. Sci.* **1998**, *67*, 87.
(22) Liu, X.; Wu, Q. *Polymer* **2001**, *42*, 10013.
(23) Nam, P. H.; Maiti, P.; Okamoto, M.; Kotaka, T.; Hasegawa, N.; Usuki, A. *Polymer* **2001**, *42*, 9633.
(24) Usuki, A.; Kawasumi, M.; Kojima, Y.; Okada, A.; Kurauchi, T.; Kamigaito, O. *J. Mater. Res.* **1993**, *8*, 1174.
(25) Usuki, A.; Kojima, Y.; Kawasumi, M.; Okada, A.; Fukushima, Y.; Kurauchi, T.; Kamigaito, O. *J. Mater. Res.* **1993**, *8*, 1179.
(26) Kojima, Y.; Usuki, A.; Kawasumi, M.; Okada, A.; Kurauchi, T.; Kamigaito, O. *J. Polym. Sci., Polym. Chem. Ed.* **1993**, *31*, 983.
(27) Yano, K.; Usuki, A.; Okada, A.; Kurauchi, T.; Kurauchi, T.; Kamigaito, O. *J. Polym. Sci., Polym. Chem. Ed.* **1993**, *31*, 2493.
(28) Kojima, Y.; Usuki, A.; Kawasumi, M.; Okada, A.; Kurauchi, T.; Kamigaito, O.; Kaji, K. *J. Polym. Sci., Polym. Phys. Ed.* **1994**, *32*, 62.
(29) Sikka, M.; Cerini, L. N.; Ghosh, S. S.; Winey, K. I. *J. Polym. Sci., Polym. Phys. Ed.* **1996**, *34*, 1443.
(30) Hasegawa, N.; Okamoto, H.; Kawasumi, M.; Usuki, A. *J. Appl. Polym. Sci.* **1999**, *74*, 3359.
(31) Lim, Y. T.; Park, O. O. *Rheol. Acta* **2001**, *40*, 220.
(32) Hoffmann, B.; Dietrich, C.; Thomann, R.; Fredrich, C.; Mülhaupt, R. *Macromol. Rapid Commun.* **2000**, *21*, 57.
(33) Ogata, N.; Kawakage, S.; Ohihara, T. *Polymer* **1997**, *38*, 5115.
(34) Liu, Y.-J.; Schindler, J. L.; DeGroot, D. C.; Kannewurf, C. R.; Hirpo, W.; Kanatzidis, M. G. *Chem. Mater.* **1996**, *8*, 525.
(35) Hyun, Y. H.; Lim, S. T.; Choi, H. J.; Jhon, M. S. *Macromolecules* **2001**, *34*, 8084.
(36) Ogata, N.; Jimenez, G.; Kawai, H.; Ogihara, T. *J. Polym. Sci., Polym. Phys. Ed.* **1997**, *35*, 389.
(37) Fournaris, K. G.; Karakassides, M. A.; Petridis, D.; Yiannakopoulou, K. *Chem. Mater.* **1999**, *11*, 2372.
(38) Krishnamoorti, R.; Giannelis, E. P. *Macromolecules* **1997**, *30*, 4097.
(39) Jimenez, G.; Okata, N.; Kawai, H.; Ogihara, T. *J. Appl. Polym. Sci.* **1997**, *64*, 2211.
(40) Pantoustier, N.; Alexandre, M.; Degée, P.; Calberg, C.; Jérôme, R.; Henrist, C.; Cloots, R.; Rulmont, A.; Dubois, P. *e-Polym.* **2001**, *9*, 1.
(41) Alexandre, M.; Beyer, G.; Henrist, C.; Cloots, R.; Rulmont, A.; Jérôme, R.; Dubois, P. *Macromol. Rapid Commun.* **2001**, *22*, 643.
(42) Alexandre, M.; Beyer, G.; Henrist, C.; Cloots, R.; Rulmont, A.; Jérôme, R.; Dubois, P. *Chem. Mater.* **2001**, *13*, 3830.
(43) Beyer, G. *Fire Mater.* **2001**, *25*, 193.
(44) Riva, A.; Zanetti, M.; Braglia, M.; Camino, G.; Flaqui, L. *Polym. Degrad. Stab.* **2002**, *77*, 299.
(45) Koopmans, R. J.; van der Linden, R.; Vansant, E. F. *J. Adhes.* **1980**, *11*, 191.
(46) Marie, E.; Chevalier, Y.; Issartel, N.; Eydoux, F.; Germanaud, L.; Flores, P. *Macromolecules* **2001**, *34*, 5838.
(47) Physical Properties Bulletin from Southern Clay Products, Inc.
(48) Han, C. D.; Jhon, M. S. *J. Appl. Polym. Sci.* **1986**, *32*, 3809.
(49) Han, C. D.; Kim, J. K. *Macromolecules* **1989**, *2*, 4292.
(50) Han, C. D.; Kim, J. *J. Polym. Sci., Polym. Phys. Ed.* **1987**, *25*, 1741.
(51) Han, C. D.; Kim, J.; Kim, J. K. *Macromolecules* **1989**, *22*, 383.
(52) Han, C. D.; Baek, D. M.; Kim, J. K. *Macromolecules* **1990**, *23*, 561.
(53) Kim, S. S.; Han, C. D. *Polymer* **1994**, *35*, 93.
(54) Han, C. D.; Kim, S. S. *Macromolecules* **1995**, *28*, 2089.
(55) Chang, S.; Han, C. D. *Macromolecules* **1997**, *30*, 1656.
(56) Lee, K. M.; Han, C. D. *Macromolecules* **2002**, *35*, 760.
(57) Solomon, M. J.; Almusallam, A. S.; Seefeldt, K. F.; Somwangthanaroj, A.; Varadan, P. *Macromolecules* **2001**, *34*, 1864.
(58) Larson, R. G. *The Structure and Rheology of Complex Fluids*; Oxford University Press: New York, 1977.

MA030302W